Cyclical Long Memory In Ship Motions At Non-Zero Speed

Vladas Pipiras, University of North Carolina, Chapel Hill, pipiras@email.unc.edu
Pavlos Zouboulоglou, University of North Carolina, Chapel Hill
Themistoklis Sapsis, Massachusetts Institute of Technology

ABSTRACT

It is common knowledge that the spectra of ship motions at non-zero speed and in following/quartering seas diverge around a fixed frequency. This work examines perhaps less known implications of this divergence on temporal dependence of motions and their squares, and on setting confidence intervals for means and variances of motions. The presented developments are largely based on what is already known and studied elsewhere in connection to the so-called (cyclical) long memory phenomenon.

Keywords: Ship motions; Wave elevation; Non-zero speed; Spectrum; Autocovariance function; (Cyclical) long memory; Confidence intervals.

1 INTRODUCTION AND MOTIVATION

This work originated from questions around the following problem. When considering ship motions in certain conditions, their sample autocorrelation functions (ACFs) happen to decay very slowly as the time lag increases. For example, Figure 1 presents one such ACF for the pitch motion from a 30-minute-long record. This is for the flared variant of the ONR Topsides Geometry Series (Bishop et al. [3]), in sea state 6, the heading of 45°, and traveling at 25 kts. The simulations were carried out through Large Amplitude Motion Program (LAMP; Lin and Yue [8], Shin et al. [11]). The lag on the horizontal axis has seconds as units. Note that the temporal dependence is quite strong at lags up to 10 minutes. In contrast, typical ACFs in many other conditions (not shown here for shortness sake) decay much faster, with the dependence visibly persisting for only 30–60 seconds.

The strong temporal dependence in Figure 1 affects downstream tasks when working with respective motions. One of the tasks is setting confidence intervals for means, variances and other basic quantities of the motions. Procedures for setting these intervals have been developed (Pipiras et al. [9]) and generally work well for ACFs with fast decay. (These will be discussed in more detail below.) But when dependence is strong, we find that the same procedures no longer work. Part of the motivation for this study was precisely this question of setting confidence intervals in the presence of strong temporal dependence as in Figure 1.

How does strong temporal dependence arise? How does one set confidence intervals in this scenario? Is there an underlying mathematical theory supporting the methodology? These are the questions addressed in this work. Some of their aspects will not be resolved completely, but we believe that this work points in the right directions and opens doors for interesting future investigations. What will be presented below is relatively well-known in statistics (especially time series), signal processing and other communities, but might be less known in naval architecture.

More specifically, in Section 2 and Appendix A, we recall first the effect of non-zero speed

on spectra of ship motions and wave elevation. It is known that the spectra diverge around certain fixed frequency. Implications of this divergence on autocovariance function (ACVF) of motions and their squares are probably less known, but can be found in Section 3. How the resulting spectrum and ACVF are affected by the underlying spectrum and speed is examined in Section 4. Implications for estimation of means and variances of motions are discussed in Section 5. A simulation study is presented in Section 6. We conclude with Section 7.

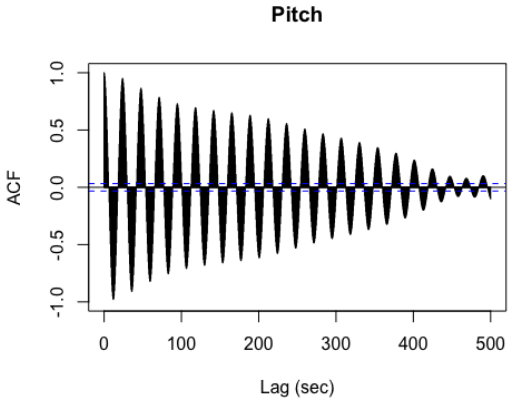

Figure 1: Autocorrelation of pitch motion.

2 LINEAR SHIP MOTIONS AND WAVE ELEVATION AT NON-ZERO SPEED

We shall assume a linear stationary regime for ship motions and underlying wave excitation. We will be switching back and forth from the time to frequency domain, using the following quantities and relations. A stationary process $X = \{X_t\}_{t\in\mathbb{R}}$ has constant mean $\mu_X = \mathbb{E}\, X_t$ and its ACVF

$$R_X(h) = \mathbb{E}\, X_t X_{t+h} - \mu_X^2 \tag{1}$$

depends on lag $h \in \mathbb{R}$ alone. The spectrum (spectral density) of X is defined as

$$\begin{aligned} S_X(w) &= \frac{1}{\pi}\int_{\mathbb{R}} e^{-iwh} R_X(h)dh \\ &= \frac{2}{\pi}\int_0^\infty \cos(wh) R_X(h)dh, \quad w \in \mathbb{R}, \end{aligned} \tag{2}$$

and satisfies

$$\begin{aligned} R_X(h) &= \frac{1}{2}\int_{\mathbb{R}} e^{ihw} S_X(w)dw \\ &= \int_0^\infty \cos(hw) S_X(w)dw. \end{aligned} \tag{3}$$

Let $\zeta = \{\zeta_t\}_{t\in\mathbb{R}}$ denote a stationary wave height process, having the (point) spectrum $S_\zeta(w)$. Let $Y = \{Y_t\}_{t\in\mathbb{R}}$ denote any of the resulting ship motions, having the spectrum $S_Y(w)$. In the linear regime and at zero speed, we have

$$S_Y(w) = |\Phi_Y(w)|^2 S_\zeta(w), \tag{4}$$

where $|\Phi_Y(w)|^2$ is the squared modulus of the transfer function (RAO), and by (3),

$$R_Y(h) = \int_0^\infty \cos(hw) S_Y(w)dw. \tag{5}$$

In the case of non-zero forward speed, the relation (5) generalizes to

$$R_Y(h) = \int_0^\infty \cos(hw_e) S_Y(w)dw, \tag{6}$$

where

$$w_e = w - qw^2 = w - \frac{U_0}{g}\cos\mu_0 w^2 \tag{7}$$

is the encounter frequency with speed U_0, heading μ_0 and acceleration g due to gravity. These developments are well-known, appear in the Principles of Naval Architecture (Lewis [7]) and other textbooks, and go back at least to Denis and Pierson [4].

Henceforth, we focus on the case

$$\mu_0 \in (-\frac{\pi}{2}, \frac{\pi}{2}) \;\Leftrightarrow\; q > 0, \tag{8}$$

that is, following or stern-quartering seas. By making suitable changes of variables, one can rewrite (6) in the form (3) as

$$R_Y(h) = \int_0^\infty \cos(h\nu)\widetilde{S}_Y(\nu)d\nu, \tag{9}$$

where $\widetilde{S}_Y(\nu)$ is the true spectrum of Y (as opposed to S_Y in (6) sometimes referred to as

pseudo-spectrum). As shown in Appendix A, we have:

$$\widetilde{S}_Y(\nu) = \frac{S_Y(w_1(\nu)) + S_Y(w_2(\nu))}{(1-4q\nu)^{1/2}} + \frac{S_Y(w_3(\nu))}{(1+4q\nu)^{1/2}}, \quad (10)$$

for $\nu \in (0, 1/4q)$, where $w_j(\nu)$, $j = 1, 2, 3$, are given in (43)–(45), and

$$\widetilde{S}_Y(\nu) = \frac{S_Y(w_3(\nu))}{(1+4q\nu)^{1/2}}, \quad (11)$$

for $\nu \in (1/4q, \infty)$.

Note that according to (10), since $w_1(1/4q) = w_2(1/4q) = 1/2q$ and if $S_Y(1/2q) \neq 0$, $j = 1, 2$, the spectrum $\widetilde{S}_Y(\nu)$ diverges as $\nu \uparrow 1/4q$. The divergence is well-recognized and is illustrated in the Principles of Naval Architecture (Lewis [7], p. 89). But consequences of this divergence may not be as known, and are discussed in the next sections.

Remark. Taking $|\Phi_Y(w)| \equiv 1$ in (4), the discussion above applies for the encountered wave height itself, which we will use for illustrations here and below. Consider, for example, the Bretschneider spectrum with a significant wave height of 7.5 meters, a modal wave period of 15 seconds, corresponding to sea state 7. Take the heading of $\mu_0 = 0$ degrees and speed of $U_0 = 12$ knots. Figure 2 depicts the original (pseudo) Bretschneider spectrum and the true spectrum transformed according to (10)–(11). The true spectrum diverges around the value $\nu = 0.433$, with the divergence depiction limited by the chosen resolution on the horizontal axis.

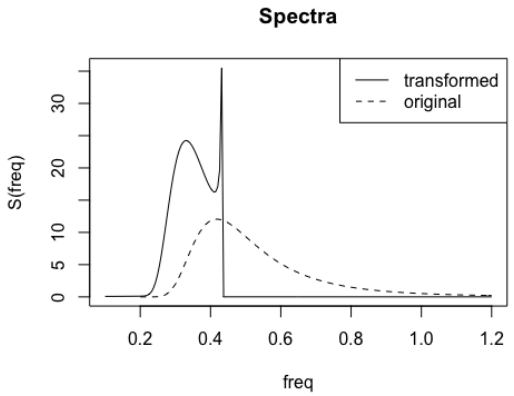

Figure 2: Transformed (true) and original (pseudo) spectra for wave elevation.

3 IMPLICATIONS FOR AUTOCOVARIANCES OF MOTIONS AND THEIR SQUARES

We shall indicate here several implications of the divergence of the spectrum around a fixed frequency in (10) for dependence in the time domain. We shall employ arguments lacking full rigor but will also point to sources with more formal derivations in special cases. Following (10), consider the case of a spectrum $S(\nu)$ satisfying

$$S(\nu) \simeq C(\nu_0 - \nu)^{-2\delta}, \text{ as } \nu \uparrow \nu_0, \quad (12)$$

where $\delta \in (0, 1/2)$ and $\nu_0 > 0$ is fixed. In the case (10),

$$\delta = \frac{1}{4}, \quad (13)$$

but it will be instructive to keep (12) more general. Note also that $\delta > 0$ ensures the divergence of $S(\nu)$, and $\delta < 1/2$ its integrability around $\nu = \nu_0$.

Turning to the time domain, consider the integral defining R through (3) around the frequency ν_0. Observe that, for small fixed $\epsilon > 0$,

$$\int_{\nu_0-\epsilon}^{\nu_0} e^{ih\nu} S(\nu) d\nu \simeq C \int_{\nu_0-\epsilon}^{\nu_0} e^{ih\nu} (\nu_0 - \nu)^{-2\delta} d\nu$$

$$= C e^{ih\nu_0} \int_0^{\epsilon} e^{-ihz} z^{-2\delta} dz$$

$$= C e^{ih\nu_0} h^{2\delta-1} \int_0^{\epsilon h} e^{-ix} x^{-2\delta} dx, \quad (14)$$

after making the changes of variables $\nu = \nu_0 - z$ and $hz = x$. As $h \to \infty$,

$$\int_0^{\epsilon h} e^{-ix} x^{-2\delta} dx \to \int_0^{\infty} e^{-ix} x^{-2\delta} dx =: A_\delta, \quad (15)$$

where the latter integral A_δ is well-defined as an indefinite integral and, in fact, can be evaluated explicitly (Gradshteyn and Ryzhik [6], Formulas 3.761.4 and 3.761.9). Putting (14) and (15) together and writing $A_\delta = a_\delta e^{i\phi_\delta}$ in polar coordinates implies that, as $h \to \infty$,

$$\int_{\nu_0-\epsilon}^{\nu_0} e^{ih\nu} S(\nu) d\nu \simeq C a_\delta e^{i(h\nu_0+\phi_\delta)} h^{2\delta-1}. \quad (16)$$

Taking the real part of (16) suggests that under (12), the ACVF of the underlying process satisfies, as $h \to \infty$,

$$R(h) \simeq C_R \cos(\nu_0 h + \phi_\delta) h^{2\delta-1}, \quad (17)$$

where $C_R = C a_\delta$. Note that (17) implies

$$\left| \int_0^\infty R(h) dh \right| < \infty, \ \int_0^\infty |R(h)| dh = \infty. \quad (18)$$

Because of the second relation in (18) and the cyclical nature of (17), the case (17) is known in the literture as *cyclical long memory* (*long-range dependence*). In that sense, the motions (at zero speed, following/quartering seas) exhibit cyclical long memory. Note that it stands in sharp contrast to many Markovian systems where the decay of ACVF is usually exponentially fast, as opposed to algebraically slow as in (17).

In discrete time, canonical examples of processes with cyclical long memory are Gegenbauer processes. See, for example, a review paper by Dissanayake et al. [5] and references therein. Their continuous-time analogues are considered in e.g. Anh et al. [1]. For these processes, it was proved rigorously that (12) implies (17).

As we shall consider the sample variances of motions, we also need to understand the implications of (12) or (17) on the motions squared. This can be done easily assuming Gaussianity of the underlying process (not much can be done in general without this assumption). Indeed, let $R_2(h)$ denote the ACVF of the process squared. Under Gaussianity, it is known that

$$R_2(h) = 2(R(h))^2 \quad (19)$$

(e.g. Pipiras and Taqqu [10], Proposition 5.1.1). Hence, (17) implies that, as $h \to \infty$,

$$R_2(h) \simeq C_R^2 \cos^2(\nu_0 h + \phi_\delta) h^{4\delta-2}$$

$$= \frac{C_R^2}{2} h^{4\delta-2} + \frac{C_R^2}{2} \cos(2\nu_0 h + 2\phi_\delta) h^{4\delta-2}.$$

That is, as $h \to \infty$,

$$R_2(h) \simeq C_{R,2} h^{2d-1} + C_{R,2} \cos(2\nu_0 h + 2\phi_\delta) h^{2d-1}, \quad (20)$$

where

$$d = 2\delta - \frac{1}{2} \quad (21)$$

is another convenient exponent to introduce. Note that

$$\left\{ \begin{array}{l} d \in (0, \frac{1}{2}) \\ d = 0 \\ d \in (-\frac{1}{2}, 0) \end{array} \right\} \Leftrightarrow \left\{ \begin{array}{l} \delta \in (\frac{1}{4}, 1) \\ \delta = \frac{1}{4} \\ \delta \in (0, \frac{1}{4}) \end{array} \right\}. \quad (22)$$

As a consequence, we have

$$\int_0^\infty R_2(h) dh = \infty, \quad (23)$$

when $d \in (0, \frac{1}{2})$ ($\delta \in (\frac{1}{4}, 1)$) or $d = 0$ ($\delta = \frac{1}{4}$). When $d < 0$, the integral in (23) is finite. This case is known as *short memory* (*short-range dependence*). The case (23) is known as *long memory* (*long-range dependence*), and is well understood by now (e.g. Beran et al. [2], Pipiras and Taqqu [10]). In that sense, the squared motions (at zero speed, in following/quartering seas) exhibit long memory.

Remark. According to (13), the case of interest here is $d = 0$ or $\delta = 1/4$. By (22), this case is at the boundary between short and long memory. This boundary case has received less attention in the literature than the long memory case $d > 0$.

4 ROLES OF UNDERLYING SPECTRUM AND SPEED

Figure 3 illustrates the relation (17) in the standardized form of the ACF for the spectrum given in Figure 2. Note the slow decay of the ACF as lag increases – this is not a

numerical error. Note, however, that the slow decay pattern in Figure 2 is different from that in Figure 1: whereas the slow decay in the latter figure has large magnitudes (relative to the largest value of 1) over a range of lags, the magnitudes are relatively small in the former figure. In fact, this results from the interplay of the underlying spectrum and speed (and heading).

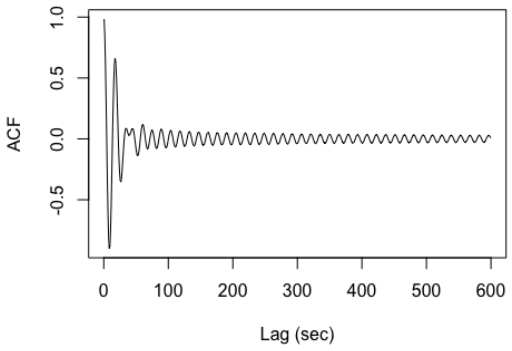

Figure 3: ACF for encountered wave elevation, having spectrum in Figure 2.

Indeed, Figures 4 and 5 present similar spectra and ACFs plots but for several speeds, 10, 13 and 15 kts. (The spectra were normalized in the plot so as to integrate to 1 or, equivalently, for the processes to have variances 1.) Note that the relative magnitudes of the ACF values is largest at 15 kts, with the pattern more akin to Figure 1. Why is that the case, and how does it relate to the shape of the spectrum?

To answer those questions, look back at Figures 2 and 3. Note that the transformed spectrum in Figure 2 consists of two components: the divergent power-law component from around the frequency $\nu = 0.4$ to $\nu = 0.433$, and the humplike component (another peak) from around the frequency $\nu = 0.2$ to $\nu = 0.4$. Denote these components as $S_d(\nu)$ and $S_h(\nu)$, and think of their sum $S_d(\nu) + S_h(\nu)$ as being the whole spectrum in Figure 2. Now, the corresponding ACVF is $R_d(u) + R_h(u)$, where R's are the

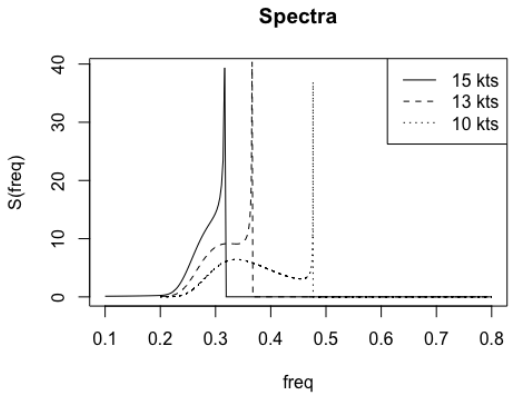

Figure 4: Spectra for encountered wave elevation at several speeds.

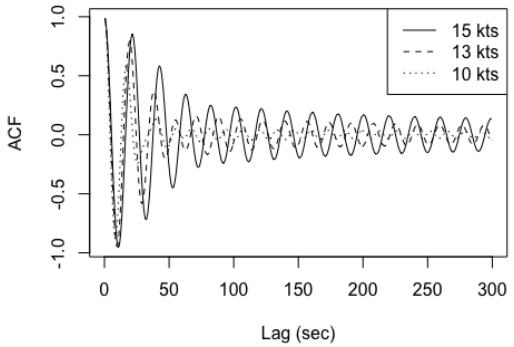

Figure 5: ACFs for encountered wave elevation at several speeds.

ACVFs of S's. If we standardized R's to ACFs so that $R(0) = 1$, the ACVF is proportional to

$$a_d R_d(u) + a_h R_h(u), \tag{24}$$

where $a_d = \int_0^\infty S_d(\nu)d\nu$, $a_h = \int_0^\infty S_h(\nu)d\nu$. In Figure 2, a_d is much smaller than a_h. The ACF $R_h(u)$ is expected to decay to 0 quickly. The ACF $R_d(u)$, on the other hand, is expected to decay slowly and have values with relatively large magnitudes. This is akin to what we see in Figures 4 and 5 for 15 kts. By combining the two observations for (24), we deduce the pattern seen in Figure 3.

Said differently, we emphasize that the slow decay in (17) is present for any $q > 0$, that is, *any* non-zero speed. Whether the slow

decay of the ACF will have relatively large magnitudes across a wide range of lags, on the other hand, depends on the shape of the transformed spectrum as discussed above.

5 IMPLICATIONS FOR ESTIMATION OF MEANS AND VARIANCES

The established long memory in (23) has implications for setting confidence intervals for the variances. To get to that point, we shall take a slightly broader path and make additional comments. Both the sample mean and variance of motion Y involve averaging

$$\overline{X}_T = \frac{1}{T}\int_0^T X_s ds, \tag{25}$$

where T is the observation window length (with $X_s = Y_s$ for mean, and in addition $X_s = Y_s^2$ for variance). In practice, the integral in (25) is discretized. The confidence interval for the mean $\mu_X = \mathbb{E}\, X_s$ is usually determined by the variability of $\mathrm{Var}(\overline{X}_T)$. The latter can be computed as

$$\mathrm{Var}(\overline{X}_T) = \frac{2}{T}\int_0^T (1 - \frac{h}{T}) R_X(h) dh \tag{26}$$

(e.g. Pipiras et al. [9]). Note that when $\int_0^\infty R_X(h)dh$ is finite, the relation (26) becomes: for large T,

$$\mathrm{Var}(\overline{X}_T) \simeq \frac{2}{T}\int_0^\infty R_X(h) dh. \tag{27}$$

The quantity $\Pi_X = 2\int_0^\infty R_X(h)dh$ is known as the *long-run variance*, and there are methods to estimate it in practice as $\widehat{\Pi}_X$ (e.g. Pipiras et al. [9]). The confidence interval for μ_X is then set as

$$\overline{X}_T \pm b_\alpha \frac{\widehat{\Pi}_X^{1/2}}{T^{1/2}}, \tag{28}$$

where b_α is a critical value at confidence level α (e.g. 1.96 at $\alpha = 0.95$ or 95% confidence level in the normal case). As the long-run variance Π_X is finite for cyclical long memory by (18), this would be the confidence interval to use in that case.

But the situation is more involved when $X = Y^2$ is the square of the motion because the long-run variance can now be infinite by (23). The behavior of (26) can nevertheless be analyzed in this case as well, and we will do so only when $\delta = 1/4$ ($d = 0$) as suggested by the ship motions application.

Asymptotic approach

We may focus just on the first term in the last expression of (20) and assume that, for large h,

$$R_X(h) \simeq C_2 h^{-1}, \tag{29}$$

since for the second term, $\int_1^\infty \cos(2\nu_0 h + \phi_\delta) h^{-1} dh$ is finite. Then, under (29), (26) becomes, for large T,

$$\mathrm{Var}(\overline{X}_T) \simeq \frac{2C_2}{T}\int_1^T h^{-1} dh - \frac{2C_2}{T},$$

that is,

$$\mathrm{Var}(\overline{X}_T) \simeq \frac{2C_2 \log T}{T}. \tag{30}$$

This suggests to set the confidence interval as

$$\overline{X}_T \pm b_\alpha \frac{(2\widehat{C}_2 \log T)^{1/2}}{T^{1/2}}, \tag{31}$$

where $\widehat{C}_2$ estimates C_2 and b_α is a suitable critical value as in (28). Note the presence of the additional term $(\log T)^{1/2}$ in (31), compared to the more conventional cases of just having $T^{1/2}$ as in (28). Estimation of the constant C_2 is discussed below.

Refined approach

The confidence intervals (31) will not be satisfactory (in fact, too narrow) in the cases where the magnitudes of ACVF values are large as in Figure 1 (or Figure 5 with 15 kts). The issue is with the asymptotic nature of (30) as follows. To simplify the exact relation (26) slightly, write

$$\mathrm{Var}(\overline{X}_T) \simeq \frac{2}{T}\int_0^T R_X(h) dh$$

$$= \frac{2}{T}\int_0^{T_0} R_X(h)dh + \frac{2}{T}\int_{T_0}^{T} R_X(h)dh \quad (32)$$

for fixed T_0. The same argument as for (30) can be made to write

$$\mathrm{Var}(\overline{X}_T) \simeq \frac{2}{T}\int_0^{T_0} R_X(h)dh + \frac{2C_2\log(T/T_0)}{T}. \quad (33)$$

For fixed T_0, the second term in (33) will dominate the first term for large T because of the extra factor $\log T$. However, for finite T, especially when the magnitudes of the ACVF values are relatively large, the first term in (33) can not be discarded. Put differently, the relation (29) used for all h's in the asymptotic approach is not a good approximation to ACVF for smaller h's. This suggests to estimate the variance of the sample mean through

$$\widehat{V}_T := \frac{2}{T}\int_0^{T_0} \widehat{R}_X(h)dh + \frac{2\widehat{C}_2\log(T/T_0)}{T} \quad (34)$$

for some fixed T_0, and set the confidence interval as

$$\overline{X}_T \pm b_\alpha \widehat{V}_T^{1/2}, \quad (35)$$

where b_α is a suitable critical value.

The term $\widehat{R}_X(h)$ in (34) should estimate the ACVF $R_X(h)$. When $X = Y^2$ and Y is consistent with the assumption of Gaussianity, in view of (19), we suggest setting

$$\widehat{R}_X(h) = 2(\widehat{R}_Y(h))^2, \quad (36)$$

as opposed to estimating the ACVF directly for $X = Y^2$. The reason is that for a Gaussian process Y, the direct estimation of the ACVF of Y^2 is rather biased downwards. This is illustrated in Figure 6 plotting the ACVF of a wave height squared $X = Y^2$ in the same conditions as for Figure 1, estimated directly and through the formula (36). Because of the downward bias, if direct estimation is used, the estimated variance in (34) will be too small and the resulting confidence interval in (35) be too narrow. Note that this is particularly acute for slowly-decaying ACVFs with relatively large magnitudes, since the biases accumulate across a range of h's.

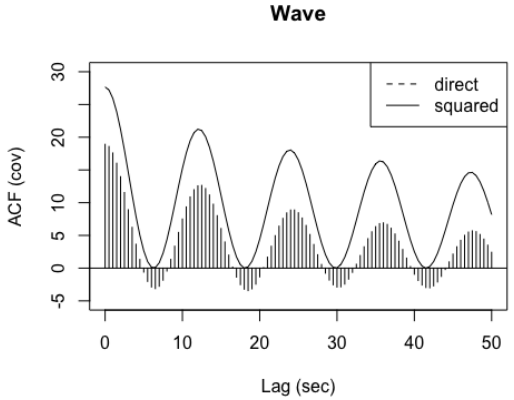

Figure 6: The ACVF of a wave height squared $X = Y^2$, estimated directly and through the formula (36).

Estimation of C_2

How could one estimate the constant C_2 in (29)? For similar problems in the long memory context, it is known and not advisable to do this in the time domain. A better practice is to translate (29) to the spectral domain, and to estimate C_2 therein. In view of (2), we expect that as $w \to 0$,

$$S_X(w) \simeq \frac{2C_2}{\pi}\int_1^\infty \cos(wh)h^{-1}dh$$

$$= \frac{2C_2}{\pi}\int_w^\infty \cos(z)z^{-1}dz \simeq \frac{2C_2}{\pi}(-\log w). \quad (37)$$

That is, the spectrum of X diverges around $w = 0$ as $(-\log w)$.

In practice, the relation (37) suggests to estimate C_2 as

$$\widehat{C}_2 = \widehat{C}_2(m) = \frac{\pi}{2}\frac{\sum_{k=1}^m \widehat{S}_X(w_k)}{\sum_{k=1}^m(-\log w_k)}, \quad (38)$$

where $\widehat{S}_X(w_k)$ are estimated spectrum values over a grid of frequencies $w_1, \ldots, w_m$ close to 0. (In practice, for discrete data, w_k's are taken as the Fourier frequencies.) The choice of m and the performance of confidence intervals (35) are examined in the next section.

6 SIMULATION STUDY

We assess here the performance of the proposed confidence intervals (35) through a simulation study, as well as discuss a number of related issues. We focus on the pitch motion and consider the same setting as in Figure 1. In the dataset we work with, there are 10,000 records of motions, each 30-minutes long. We use all records to calculate what we consider the true variance of pitch. The true variance is used to check the performance of confidence intervals constructed for individual records. If the confidence intervals work well, they should capture the true variance around the number of times which corresponds to the confidence level of the confidence intervals. E.g. with 95% confidence interval and 100 records, we expect that number to be close to 95. The proportion of times will be referred to as a passing rate.

Figure 7 presents the proposed confidence intervals for the first 100 records. Each circle point is the actual record variance and the vertical line is the associated 95% confidence interval. The horizontal line represents the true variance. The passing rate is 0.91. It suggests that the confidence intervals are slightly anti-conservative but still perform reasonably well.

The passing rate should be contrasted with the following two alternatives. When using the confidence intervals where the variance (32) includes only the first term (that is, one does not account for long memory), the passing rate is 0.86. Furthermore, when using the same approach but estimating the ACVF $R_X(h)$ directly from $X = Y^2$ (cf. Figure 6), the passing rate drops to 0.72.

Finally, we comment on the choice of the two parameters T_0 and m entering into calculating the confidence intervals (35), with m through the estimator $\widehat{C}_2$ in (38). In the results above, we took $T_0 = 200$ seconds. This choice should be driven by the range of lags where the ACVF is believed to be estimated well. Our results though were not very sensitive to taking a larger value of T_0. For the choice of m, we examined $\widehat{C}_2(m)$ as a function of m for several records. As presented in Figure 8 for 5 records, they share a similar pattern, where looking from the right to the left, the values slowly increase before stabilizing and having more variability. More variability is expected since the averages in (38) involve fewer terms for smaller m. One is interested in the region where the estimates stabilize because (37) is an asymptotic relation, so that the estimation of $\widehat{C}_2(m)$ will naturally have bias for larger m. In the results above, we took $m = 10$.

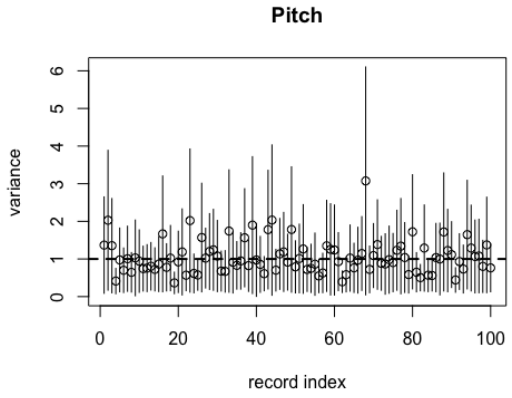

Figure 7: Confidence intervals for the pitch variance over 100 records. The horizontal line represents the true variance.

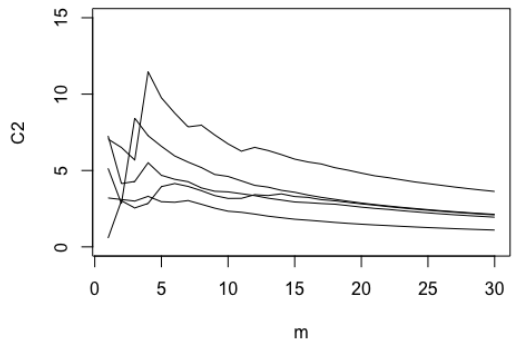

Figure 8: Estimates $\widehat{C}_2(m)$ versus m for 5 records.

7 CONCLUSIONS

In this work, we focused on motions whose ACFs decay very slowly as in Figure 1. We explained how this behavior arises from non-zero speed and the underlying spectrum of the motion at zero speed, making connections to the phenomenon of (cyclical) long memory. Finally, we discussed implications of these findings on constructing confidence intervals for the variances of motions with slowly decaying ACFs.

Acknowledgments

This work has been funded by the Office of Naval Research grant N00014-19-1-2092 under Dr. Woei-Min Lin. The authors also thank Dr. Vadim Belenky at NSWCCD for raising and discussing the problem addressed in this work, and for providing the test dataset of motions.

References

[1] V. Anh, V. Knopova, and N. Leonenko. Continuous-time stochastic processes with cyclical long-range dependence. *Australian & New Zealand Journal of Statistics*, 46(2):275–296, 2004.

[2] J. Beran, Y. Feng, S. Ghosh, and R. Kulik. *Long-Memory Processes*. Springer, 2013.

[3] R. Bishop, W. Belknap, C. Turner, B. Simon, and J. Kim. Parametric investigation on the influence of GM, roll damping, and above-water form on the roll response of model 5613. Technical report, NSWCCD-50-TR-2005/027, Hydromechanics Department, Naval Warfare Center Carderock Division, West Bethesda, Maryland, 2005.

[4] M. Denis and W. Pierson. On the motions of ships in confused seas. *The Transactions of the Society of Naval Architects and Marine Engineers*, 61:280–357, 1953.

[5] G. Dissanayake, M. Peiris, and T. Proietti. Fractionally differenced Gegenbauer processes with long memory: A review. *Statistical Science*, 33(3):413–426, 2018.

[6] I. Gradshteyn and I. Ryzhik. *Table of Integrals, Series, and Products*. Academic Press, 2014.

[7] E. Lewis. *Principles of Naval Architecture Second Revision, Volume III (Motions in Waves and Controllability)*. The Society of Naval Architects and Marine Engineers, Jersey City, NJ, 1989.

[8] W.-M. Lin and D. Yue. Numerical solutions for large amplitude ship motions in the time-domain. In *Proceedings of the 18th Symposium on Naval Hydrodynamics*, Ann Arbor, 1991.

[9] V. Pipiras, D. Glotzer, V. Belenky, M. Levine, and K. Weems. On confidence intervals of mean and variance estimates of ship motions. In *Proceedings of the 13th International Conference on the Stability of Ships and Ocean Vehicles*, Kobe, Japan, 2018.

[10] V. Pipiras and M. Taqqu. *Long-Range Dependence and Self-Similarity*. Cambridge University Press, 2017.

[11] Y. Shin, V. Belenky, W. Lin, K. Weems, and A. Engle. Nonlinear time domain simulation technology for seakeeping and wave-load analysis for modern ship design. authors' closure. *Transactions os the Society of Naval Architects and Marine Engineers*, 111:557–583, 2003.

A Derivation of spectrum

The goal here is to relate the pseudo-spectrum S_Y and the true spectrum $\widetilde{S}_Y$ as

$$\int_0^\infty \cos((w - qw^2)h) S_Y(w) dw$$

$$= \int_0^\infty \cos(\nu h)\widetilde{S}_Y(\nu)d\nu, \qquad (39)$$

and to derive the expressions (10)–(11). Given the form of the encounter spectrum $w_e = w - qw^2$ and the assumption $q > 0$ in (8), write the left-hand side of (39) as the sum of three integrals over

$$\left(\int_0^{1/2q} + \int_{1/2q}^{1/q} + \int_{1/q}^{\infty}\right) \ldots dw = \sum_{j=1}^{3} I_j.$$

The changes of variables $\nu = w - qw^2$ for the first and second integrals, and $-\nu = w - qw^2$ for the third integral have unique solutions $w = w(\nu)$ defined below, and allow to express the integrals as

$$I_1 = \int_0^{1/4q} \cos(\nu h) S_Y(w_1(\nu)) \frac{dw_1}{d\nu} d\nu, \qquad (40)$$

$$I_2 = \int_0^{1/4q} \cos(\nu h) S_Y(w_2(\nu)) (-\frac{dw_2}{d\nu}) d\nu, \qquad (41)$$

$$I_3 = \int_0^{\infty} \cos(\nu h) S_Y(w_3(\nu)) \frac{dw_3}{d\nu} d\nu, \qquad (42)$$

where

$$w_1(\nu) = \frac{1}{2q}(1 - (1 - 4q\nu)^{1/2}), \qquad (43)$$

$$w_2(\nu) = \frac{1}{2q}(1 + (1 - 4q\nu)^{1/2}), \qquad (44)$$

$$w_3(\nu) = \frac{1}{2q}(1 + (1 + 4q\nu)^{1/2}). \qquad (45)$$

Differentiating (43)–(45) and gathering all the terms in (40)–(42) leads to (39) with $\widetilde{S}_Y$ given by (10)–(11).